Physical principles of microwave assisted magnetic recording

Kirill Rivkin, Mourad Benakli, Ned Tabat, and Huaqing Yin

Articles you may be interested in

Microwave-assisted magnetic recording simulation on exchange-coupled composite medium
J. Appl. Phys. 111, 07B711 (2012); 10.1063/1.3678450

Microwave-assisted magnetic recording at lower transverse oscillating field
J. Appl. Phys. 105, 07B908 (2009); 10.1063/1.3089492

Domain wall assisted magnetic recording (invited)
J. Appl. Phys. 101, 09K108 (2007); 10.1063/1.2714271

Domain wall assisted magnetic recording
Appl. Phys. Lett. 89, 062512 (2006); 10.1063/1.2335590

Physics of patterned magnetic medium recording: Design considerations
J. Appl. Phys. 98, 024505 (2005); 10.1063/1.1977192

Physical principles of microwave assisted magnetic recording

Kirill Rivkin,[1] Mourad Benakli,[1] Ned Tabat,[2] and Huaqing Yin[1]
[1]*Seagate Technology, Edina, Minnesota 55435, USA*
[2]*Semaphore Scientific Inc., Chanhassen, Minnesota 55317, USA*

While the basic physics of Microwave Assisted Magnetization Reversal (MAMR) phenomenon is well established both theoretically and experimentally, its application in a practical magnetic recording environment was so far studied primarily with the help of micromagnetic recording models. In this work, we instead attempt to use analytical formulation and simple numerical models to understand the main challenges as well as benefits that are associated with such a system. It appears that the main difference between the previously introduced theory [G. Bertotti *et al.*, Phys. Rev. Lett. **86**, 724 (2001); K. Rivkin *et al.*, Appl. Phys. Lett. **92**, 153104 (2008); S. Okamoto *et al.*, J. Appl. Phys. **107**, 123914 (2010).] and recording environment is that both the RF and DC magnetic fields are applied at a substantial angle to the anisotropy axis. While the associated symmetry breaking prevents one from describing the reversal process explicitly, it is possible to approximate the solutions well enough to satisfactorily match numerical models both in the case of wire and Spin Torque Oscillator generated RF fields. This approach allows for physical explanation of various effects associated with MAMR such as high gradient of writeable anisotropy and reduction of track width, and offers a clear guidance regarding future optimization of MAMR recording. © *2014 AIP Publishing LLC*. [http://dx.doi.org/10.1063/1.4882063]

Microwave Assisted Magnetization Reversal (MAMR) is a phenomenon where RF frequency field is applied to magnetic material and by resonantly exciting large angle precessions succeeds in lowering its coercivity, or even reversing the magnetization altogether. The existence of such effect was first proposed in 1970s, but it was not researched in any depth until rediscovered independently by a number of groups in 2000s. One of the first papers on the subject presented the experiment which clearly demonstrated the phenomenon by applying a combination of RF and DC fields to magnetic nanoparticles and observing the reduction of their switching field.[1] Later, a simple theory of the phenomenon was developed,[2] which assumes that the magnetic body can be described as a single spin, i.e., its magnetization remains mostly uniform during the switching, which is likely to be true for all sufficiently small samples, smaller or comparable to the exchange length. This includes the ones of considerable practical interest: ferromagnetic nanoparticles on 10 nm scale or grains in magnetic granular recording media. It was shown that as one investigates the possible modes of precession that can lead to a magnetization reversal, one needs to fulfill the condition that there are no stable modes with small precessing angles,[2,3] i.e., the magnitude of the RF field is large enough so that all of them become unstable. RF induced switching path is then somewhat similar to a Lyapunov stable analytical solution which can be obtained for the case when the RF frequency is a function of time[4] and the increase of effective magnetic field (or reduction in the media's coercivity) can be expressed in terms of appearance of an extra field component linearly proportional to the RF frequency.[5]

Analytical solutions are available when the RF field polarization is circular, i.e., when the RF field rotates around the anisotropy axis, so that the phase difference between the rotating magnetization and the RF field is constant, but they can be readily extended towards the case of linearly polarized field by just reducing its amplitude by half. The explanation is that linearly polarized field is equivalent to two circularly polarized components with opposite chiralities: one acts in resonance when the magnetization is close to its initial state, and the other one acts in anti-resonance and therefore becomes relevant only when the magnetization is close to being reversed.[3] This means that unlike purely circular polarization, which can in theory reverse the magnetization all by itself, linear polarization can only push the magnetization to the point where its projection on anisotropy axis is zero; going any further will activate MAMR effect which will pump the energy into the system and move the magnetization back towards zero. However, if a large DC field is simultaneously applied, the resonant frequency when magnetization is parallel to the DC field is increased, while that for the opposite case—decreased and therefore a higher frequency can still cause the magnetization reversal. Using the analytical solution with half the magnitude of the RF field then becomes justifiable.

How applicable are such single spin models? Thankfully, there is a large body of experimental work,[6–8] which clearly demonstrates MAMR effect on a large variety of magnetic materials. In particular, three things become apparent:

a. Thermal contribution to switching probability becomes substantial for long (many tens or hundreds of nanoseconds) RF pulses, but does not seem to alter MAMR effect on shorter time scale and on a timescale of recording processes (100–300 ps) is likely to be negligible.

b. Large objects (i.e., with dimensions substantially exceeding the exchange length) can exhibit a dramatically enhanced MAMR effect.[9] The proposed explanation is excitation of non-uniform modes; the similarity should be noted with modeling of the media with partially exchange decoupled layers, where a similarly large enhancement was found.[10,11]

c. Most importantly, single spin theory offers a rather good prediction of the switching field as a function of the applied frequency; the observed reduction of coercivity and the optimal frequency are both slightly larger than the analytical limit, which can be taken into account by a minor adjustment in the formulas, as shown below in this paper.

The last observation also addresses the possible impact of damping on MAMR effect. Obviously, increased damping constant means more energy transferred from the RF field to heat rather than magnetization precession and results in overall reduction of MAMR effect, even though as magnetization becomes aligned with the direction of the DC magnetic field it relies on damping to speed up the reversal process. At the same time, it is extremely uncertain *a priori* which value of damping should be used in a single spin formalism. It has been long speculated, that when majority of the reversal occurs at relatively high angle with respect to the equilibrium, a nonlinear damping coefficient should be employed.[12] One also should consider the effect of multi-magnon scattering, especially for larger systems.[13]

However, what MAMR experiments demonstrate, is that despite being performed on materials where the physics of damping processes varies significantly (ranging from permalloy films[8] to continuous modern recording media[7] or high anisotropy dots of various sizes[9]), there are no cases where the damping negates the MAMR effect or requires substantial alteration of analytical formulas, even though in deriving the latter the damping term was omitted altogether.[2] In the most severe case, which is excitation of non-uniform magnetization, it actually enhances the MAMR effect.[9] In all other cases, it appears that to sufficiently well describe the system is to enough to use a value of damping coefficient of $\beta = 0.06$ or thereabout. It can be shown that for such values of damping, the formalism[2] can be altered by introducing a relatively minor reduction of the amplitude of the RF field, linearly proportional to the damping coefficient.

In all these experiments, the DC field is anti-parallel to the initial direction of magnetization and the RF field is perpendicular to the anisotropy axis. Let us consider how this differs from a typical magnetic recording setup.[18] At the heart of such system (Fig. 1) lies the construction which includes a non-magnetic writer gap, separating narrow magnetic pole (typically made from high saturation magnetization material, i.e., $4\pi M_s = 2.4T$) from the shield. Recording media is located below the writer, with anisotropy axis oriented perpendicular to its surface. Let us introduce the coordinate system to be used throughout this paper, in which z axis is parallel to the anisotropy axis in the media, with positive direction aligned with the initial (non-reversed) orientation of the magnetization. The DC wrier field[19] (Fig. 1) in
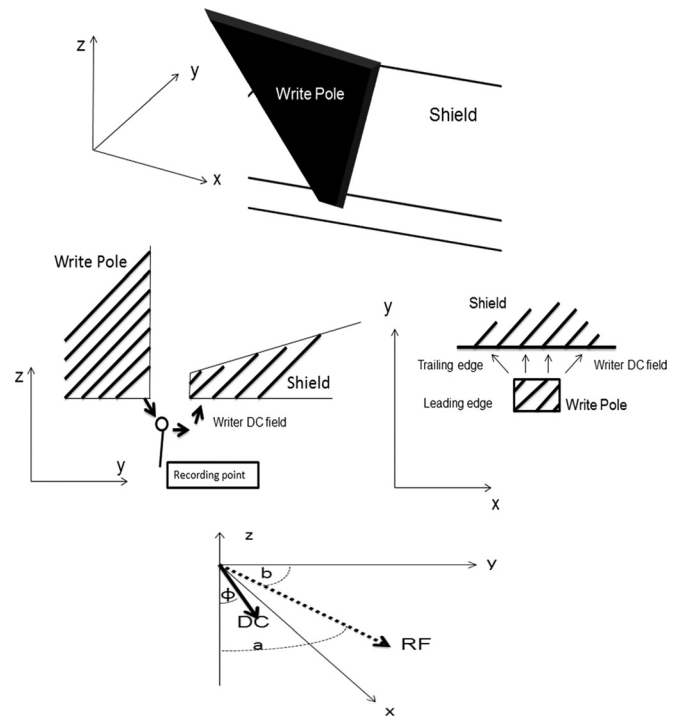

FIG. 1. Magnetic recording setup and the coordinate axis chosen with the nomenclatures for angles defining the direction of RF and DC fields.

the gap is applied along yz plane, with a negative projection on z axis. The x direction is the direction parallel to the edge of the write pole.

In the gap, magnetic field changes its angle with respect to anisotropy axis from 0° and anti-parallel to the magnetization direction (the one we want to reverse) underneath the pole (Fig. 1, zy projection) to perpendicular somewhere close to the gap's center and parallel to both anisotropy axis and magnetization direction—at the end of the gap (where no magnetization reversal occurs). In the Stoner-Wolfarth limit,[14] the highest anisotropy value can be written when the anisotropy axis and magnetic DC field are at 45° with each other—which occurs in the gap, close to the write pole. After this, towards the shield, the capability of magnetic field to reverse magnetization quickly drops. Resulting high gradient of writeability, i.e., the fact that the maximum writeable anisotropy (which we further on characterize by corresponding value of anisotropy field H_k) varies fast within the gap is very important. This gradient along the y axis, together with the width of the write field (which depends on the gradient along x axis, Fig. 1, xy projection) define the maximum achievable areal density.

Before we discuss performance of MAMR system, let us briefly indicate the parameters that define magnetic recording in general. First, it is the amplitude of energy barrier that separates two possible magnetization states in the media (i.e., the ones when the magnetization is parallel to the anisotropy axis). For sufficiently small values of it, the magnetization becomes thermally unstable (on timescale of months or a few years) and therefore unusable for reliable information storage. This means that the absolute value of media H_k (as determined by the strength of the writer field), multiplied by the grain's volume is a constant independent on writer

design. Any boost of writer field and H_k can then be converted to improved areal density (at least theoretically), by decreasing the media grain size and therefore—*increasing* number of grains per written "bit," resulting in higher signal to noise ratio.

In a more general case, one can achieve higher areal density either by reducing the track width, while maintaining or slightly improving both the maximum writeable H_k and the writeability gradient or by substantially increasing both the maximum writeable H_k and the writeability gradient, while simultaneously reducing the grain size in the media. In the first case, one relies on improving the track density, in the second case—linear density (i.e., the number of bits in the direction of the writer head's movement, parallel to the track direction and along x axis in Fig. 1). The areal densities higher than 2 Tbit/in^2 cannot be obtained without at least some lowering of the media grain size (which means redesigning the magnetic media) and overall requires the second approach, but to advance from the current areal density limit (around 1 Tbit/in^2) (Ref. 20) the first approach is sufficient: one needs to be able to record more narrow tracks, while modestly improving other recording parameters. It is nearly impossible to do so with a conventional recording head, as reduction of the track width by, for example, reducing the width of the write pole, leads to loss of magnetic field amplitude generated by the write pole—and therefore loss of writeability and its gradient.

As we will show further on, in MAMR all these three key recording parameters—track width, writeability gradient within the gap, and the value of media anisotropy H_k—are intrinsically related, which allows for implementation of both approaches, as it can be used to simultaneously substantially reduce the track width, boost writeability and increase the gradient, although the last parameter in MAMR-assisted recording is substantially different from the one in conventional recording.

As we mentioned before, the peak writeability in a conventional recording system occurs when the DC field is at 45° with respect to the anisotropy axis—and it is reasonable to assume that this is exactly the point where we also want to maximize the MAMR effect. Unfortunately, the analytical formulas[2] in their derivation heavily rely on the fact that the problem has spherical symmetry with respect to the anisotropy axis, i.e., the DC field is parallel to the anisotropy axis. It is however possible to combine numerical and analytical approaches to further extend it. As before, we assume for the moment that the damping can be neglected.

If we take a point in the gap where the angle between the DC field and anisotropy axis is denoted by ϕ (Fig. 1, zero corresponds to the DC field anti-parallel to the initial direction of the magnetization), then the resonant frequency (more precisely, since we do not require the system to be at the equilibrium—its real component) of a configuration where the magnetization tips by the angle φ with respect to the positive z axis, while remaining in the yz plane, is given by

$$\omega = \gamma\sqrt{(H_k - H_0\cos\phi)^2 + H_0\sin\phi(H_0\sin\phi - H_k\sin\varphi)}. \tag{1}$$

H_0 is the amplitude of the DC field and H_k is the maximum anisotropy we can switch with MAMR. It is driven by both Stoner-Wolfarth component $H_{SW} = ((H_0\cos\phi)^{\frac{2}{3}} + (H_0\sin\phi)^{\frac{2}{3}})^{\frac{3}{2}}$ and MAMR enhancement, which we will further on denote as effective MAMR field H_{eff}: $H_k \approx H_{SW} + H_{eff}$.

If there would be no application of the RF field, instead of reversing, the magnetization would reach the local minimum of the energy function $E = -H_k\cos^2\phi + H_0\cos(\phi + \varphi)$. Combining this with Eq. (1) and assuming a rather crude approximation, when both φ and ϕ are relatively small, the FMR frequency of such equilibrium configuration is close to the one given as if the magnetization would not have tipped at all

$$\omega \approx \gamma(H_k - H_0\cos\phi). \tag{2}$$

If MAMR field is applied at frequency above this value, the system is off resonance and the effect is miniscule, however, the optimal MAMR frequency, for which the reduction of switching field H_{eff} is the largest—is substantially smaller. One of the ways to look at it is that while the DC field of any magnitude with non-zero ϕ will tip the magnetization by some angle (since it resides in a local energy minimum), the reversal will not happen, as the effective field needed to overcome the potential barrier given by the above mentioned expression for the potential energy is proportional to the largest derivative of such potential—the one observed at a much higher angle φ. This in part also explains why MAMR effect has limited dependence on starting conditions, or risetime of the external field:[15] it does not require the phase matching between the RF field and magnetization in the beginning of the reversal, as initial motion occurs mostly under the influence of the DC field, but when the MAMR reduction of coercivity actually occurs, synchronization between the magnetization and RF field is favored since it is the only Lyapunov stable trajectory. It can also be shown that almost the entire transfer of energy from the RF field to the system occurs in close to just 2 periods of the RF field, which means that thermal fluctuations have to be rather severe to perturb the trajectory in a significant way; however, they do have an impact of increasing the probability that magnetization switches back. Recalling the analytical solution[3] for $\varphi = 0$, in the absence of DC field and with circularly polarized RF field,

$$\frac{H_{RF}}{H_k} > \left(1 - \left(\frac{\omega}{\gamma H_k}\right)^{\frac{2}{3}}\right)^{\frac{3}{2}}; \quad \frac{H_{RF}}{H_k} > \sqrt{2}\left(\frac{\omega}{\gamma H_k}\right) - \sqrt{\frac{2}{3}}, \tag{3}$$

where H_{RF} is amplitude of RF field, H_k is anisotropy that can be reversed, ω is RF field's frequency, and γ is gyromagnetic ratio. The solution was obtained by solving the Landau-Lifshitz equation in spherical coordinates and observing the conditions for which all trajectories with a fixed phase difference between the magnetization vector and that of RF field become unstable, i.e., the energy flowing into the system is substantial enough and is in resonance with the magnetization, so that its reversal is the only valid outcome. Its transformation for the case of DC field applied parallel to the anisotropy axis is straightforward.[3,9] For a more general

case, with non-zero DC field's angle and linearly polarized RF field, assuming that the RF field is applied at the optimal angle (effect of which will be discussed shortly), the same can be done only in a very approximate fashion, yielding

$$\frac{H_{RF}}{2(H_k - H_{SW})} > \left(1 - \left(\frac{\omega}{\gamma(H_k - H_0\cos\phi)}\right)^{\frac{2}{3}}\right)^{\frac{3}{2}}$$

$$\frac{H_{RF}}{2(H_k - H_{SW})} > \sqrt{2}\left(\frac{\omega}{\gamma(H_k - H_0\cos\phi)}\right) - \sqrt{\frac{2}{3}}. \qquad (4)$$

The solution for the most optimal MAMR effect, i.e., largest value of $H_k - H_{SW}$ is given by

$$\omega \approx 0.66\gamma(H_k - H_0\cos\phi)$$

$$H_k = H_{SW} + \frac{H_{RF}}{2\left(1 - \left(\frac{\omega}{\gamma(H_k - H_0\cos\phi)}\right)^{\frac{2}{3}}\right)^{\frac{3}{2}}} \qquad (5)$$

$$\approx H_{SW} + 4.25H_{RF}.$$

Let us compare this formula with the numerical calculations. Here and after, we will extensively use the model, in which we approximate the media as a single magnetic dipole with Landau damping coefficient $\beta = 0.06$. DC and RF fields are applied as a linear function of time with the risetime of 150 ps; modeling of other risetimes revealed that the main difference is that for substantially shorter ones (<50 ps) the magnetization enters the mode of precessional switching, but even in this case (which currently holds little practicality), majority of the analysis in this paper holds after a few rather obvious adjustments. For the current state of the art magnetic recording, the risetimes exceed 100 ps. Another practical consideration is that in reality the DC field reverses its direction for the purpose of writing "up" and "down" bits, however, for this effect to have a real impact on MAMR effect as described by Eqs. (1)–(5), the field reversal should happen on 200 ps scale—faster than the value typically used in modern recording systems.

Similarly, for the purpose of this paper there is a substantial consistency between performing the modeling with and without the presence of temperature (80 °C roughly corresponds to a typical hard drive environment). Adding stochastic noise, and considering the magnetization "reversed" if a 90% or higher switching probability is established in the modeling yields qualitatively the same results as making just a single calculation without temperature and recording whether the magnetization reversal occurred.

In this first modeling run, we vary the value of the DC field angle from 10° to 80°, keep the DC field amplitude equal to 1 Tesla and that of linearly polarized RF field to 0.1 Tesla. For each value of the DC field angle, we find the RF field angle for which the switchable anisotropy is largest.

The last condition is very important, as (Eq. (5)) is a theoretical maximum of the attainable MAMR effect. In order for this value to be achieved, the projection of torque produced by the RF field, $\mathbf{m} \times \mathbf{h}_{RF}$, should be such that it is aligned along the path across the potential barrier; if the RF field were to be instead at this moment aligned parallel with

the magnetization, the MAMR effect would disappear. The optimal angle of the RF field depends on the angle of the DC field in the manner which we will consider later on in this manuscript.

Finally, we compare the results with Eq. (5). They are noticeably similar, however, just as we discussed before when addressing the discrepancies between analytics and experimental results—the optimal MAMR frequency and reversible anisotropy are both slightly higher than the ones given by (Eq. (5)). Since the correction is small, for practical purposes we believe it should be taken into account by rewriting the (Eq. (5)) as

$$\omega = 0.72\gamma(H_k - H_0\cos\phi)$$

$$H_k = H_{SW} + \frac{H_{RF}}{2\left(1 - (0.72)^{\frac{2}{3}}\right)^{\frac{3}{2}}} \approx H_{SW} + 5.8H_{RF}. \qquad (6)$$

We present the resulting comparison between the numerics and analytics given by Eq. (6) in Fig. 2. Both reversible anisotropy field H_k (thick lines) and optimal MAMR frequencies (expressed, from here onwards also in the units of corresponding magnetic field $f = \omega/\gamma$, meaning that f = 1 T roughly corresponds to 28 GHz frequency) appear to be very consistent.

Consider now a more general case when the RF field is applied in the same yz plane as anisotropy axis and the DC field, at some angle a, measured with respect to the anisotropy axis along the reversed direction of the magnetization (Fig. 1). As we mentioned before, of particular interest is the case when DC field is at about 45° (and if angle a is also at 45° this makes both fields applied in parallel). Numerically, it is easy to calculate how optimal angle of the DC field affects optimal angle of the RF field (Fig. 3). As the DC field increases, the RF field angle decreases; for almost all DC field angles of practical interest though it remains close to 57°. This means that if we were to repeat the experiment shown previously in Fig. 2 for the fixed angle instead of optimizing its value at each point, the results would be similar, provided we choose the RF field's angle to be close to 55°–60°.

Again, even though the strict mathematical derivation of the impact due to operating at a suboptimal angle is difficult, it is intuitively simple to construct an approximate expression. First and foremost, the RF field effectively decreases. The reduction is proportional to that of $\mathbf{m} \times \mathbf{h}_{RF}$, i.e., the cosign of the Δa—the difference between the chosen and the optimal (like the ones shown in Fig. 3) value of RF field's angle

$$H_k \approx H_{SW} + 5.8H_{RF}|\cos\Delta a|. \qquad (7)$$

From Eq. (3), the optimal frequency should also decrease to satisfy (Eq. (7))

$$\frac{\omega}{\gamma} \approx -1.63H_{RF} + 0.72(H_{SW} - H_0\cos\phi) + H_{eff}$$

$$\approx -1.63H_{RF} + 0.72(H_{SW} - H_0\cos\phi) + 5.8H_{RF}|\cos\Delta a|. \qquad (8)$$

Let us compare Eqs. (7) and (8) with numerical modeling, performed in the same manner as before, but for the
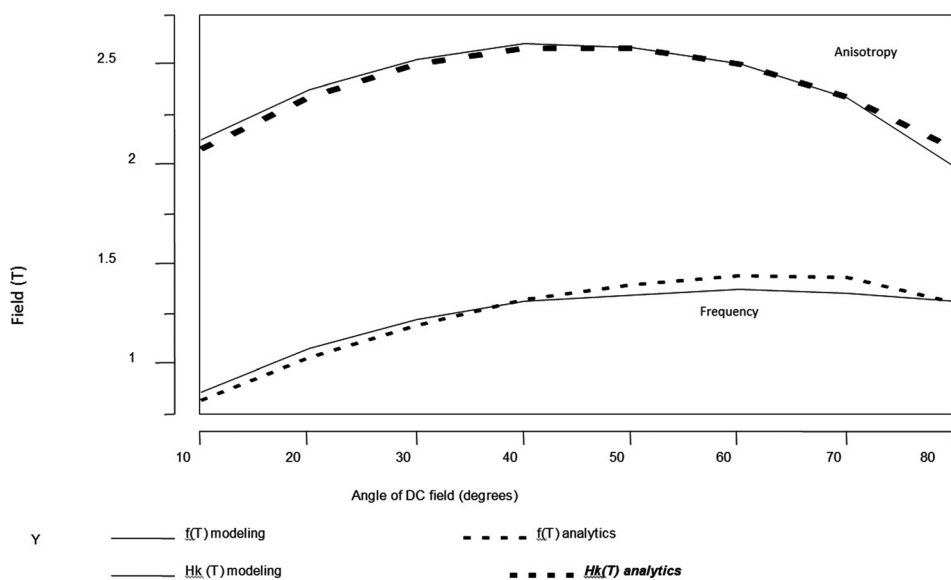
FIG. 2. Numerical (solid lines) and analytical (dashed lines) solutions for the case of angled DC field; both optimal MAMR frequency $f = \omega/\gamma$ (in units of magnetic field, T) and largest switchable anisotropy H_k are given in the unit of field, Tesla.
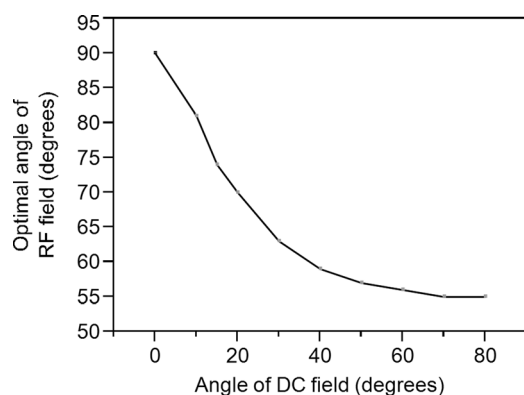

FIG. 3. The optimal angle of the RF field as the function of the DC field angle.

FIG. 4. Numerical (solid line) and analytical (dotted line) estimation of effective field $H_{eff} = H_k - H_{SW}$, for fixed DC field angle at 45° angle and varied RF field angle a.

fixed angle of the DC field (45°) and varied angle of the RF field a. As we can see, the analytics matches the numerical results very well for a wide range of angles, both in terms of optimal MAMR frequency f = ω/γ and MAMR effective field $H_{eff} = H_k - H_{SW}$ (Fig. 4). It should be noted that Eqs. (7) and (8) are most accurate when the DC field angle is in 30°–80° range—for very small DC field angles (0°–5°), the torque produced on the media magnetization in the absence of the RF field, by the DC field alone is rather small and switching is therefore significantly suppressed.

Equations (7) and (8) are rather general in nature, and in the next few paragraphs we will see them being applied to more and more practical scenarios, showing that even for a realistic MAMR system they correctly predict the magnitude of MAMR effect and its resonant frequency.

With this, let us study the case for which the RF field can be considered uniform in the recording gap in Fig. 1. This can be practically obtained if the RF field is generated by a wire placed in proximity to the recording area. Let us consider a simplification, for which in the gap the DC writer field remains constant in amplitude, but changes its angle from 0 (underneath the write pole) to 90° (at the gap's center). The RF field is applied at a constant frequency, and therefore H_{eff} will no longer be constant, but will reflect the
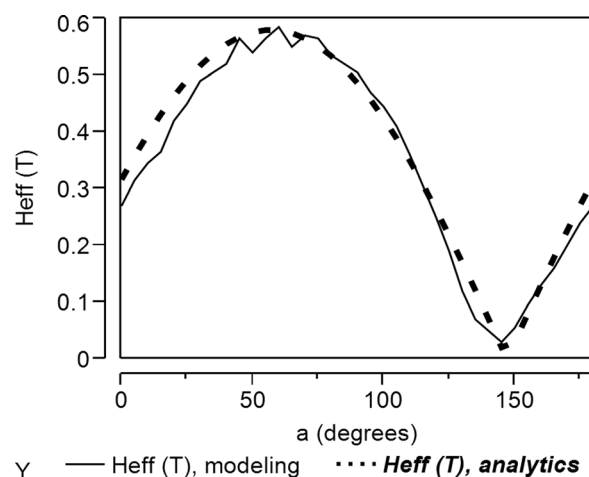
fact that the optimal MAMR frequency is a function of the DC field angle. With the modeling parameters same as before, i.e., DC field amplitude is 1 T, RF field amplitude is 0.1 T, the results are presented in Fig. 5. As the optimal frequency does not vary much in 40°–70° range (Fig. 2), the H_{eff} will also vary little. In this region, the gradient of writeability dH_{eff}/dy–change in maximum reversible anisotropy with the change of position within the gap (which corresponds to the change in the DC field angle), will be the same as for the DC field only case. Large variations in MAMR effect occur at specific angles between 0° and 30°, where correspondingly the optimal frequency varies the most (Fig. 2) and if the RF frequency is high enough—above 80°, where the optimal frequency $f = \omega/\gamma$ starts to decrease, albeit only a little bit (Fig. 2).

The reason for such a sharp change is that as was demonstrated before[2,3] the MAMR effect has a rather abrupt end in the high frequency region, where there suddenly appears a stable oscillatory mode. As the angle of the DC field changes, this cutoff frequency also shifts, as shown in Fig. 6.
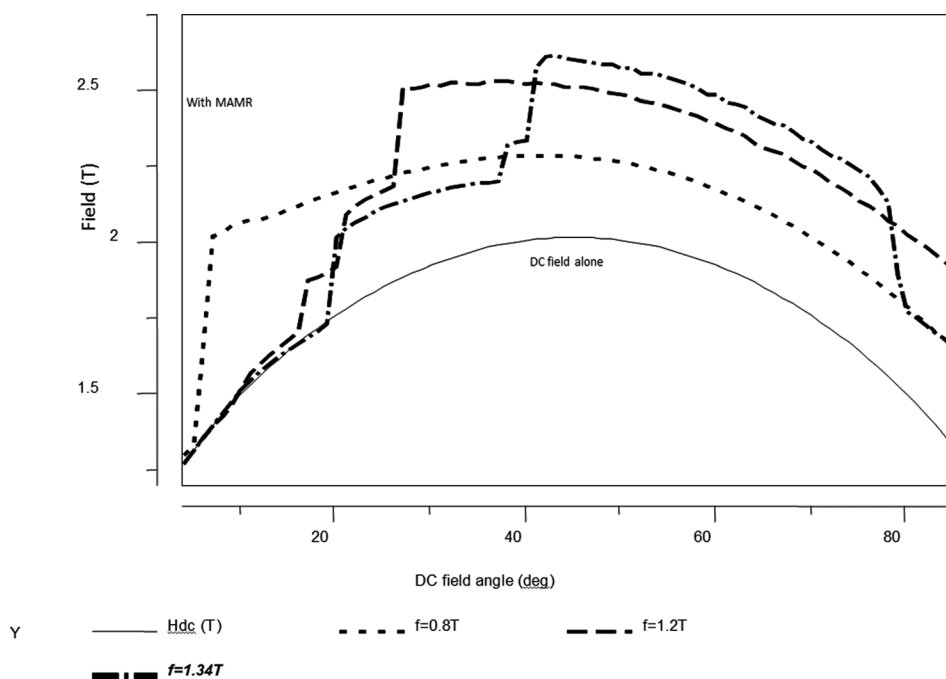
FIG. 5. Maximum reversible anisotropy as a function of DC field angle for various RF field frequencies: 0.8, 1.2, and 1.34 T. Solid line is writeable anisotropy with only the DC field.

This cutoff frequency, given by (Eq. (8)), is not only the largest for which MAMR effect is still observed, but also the optimal MAMR frequency for the given DC field angle. When the RF field is applied at this cutoff frequency we have a full MAMR enhancement of writeability at this angle, and no MAMR effect at the one only marginally different (Fig. 6). As we briefly mentioned in the previous work,[3] the transition is infinitely sharp in idealized case. By introducing temperature and substantially weakening the DC field (for example, evaluating the transition occurring at the track's edges rather than in the center), we can observe decrease of both the optimal frequency and MAMR effective field. The transition will become more probabilistic, i.e., it is the probability of switching that will vary rather than just the value of switchable anisotropy—nevertheless it will still be considerably sharply confined.

This phenomena underlies what we should call MAMR-specific gradient. Irregardless of the method by which RF field is produced, at some point there is always a drop of
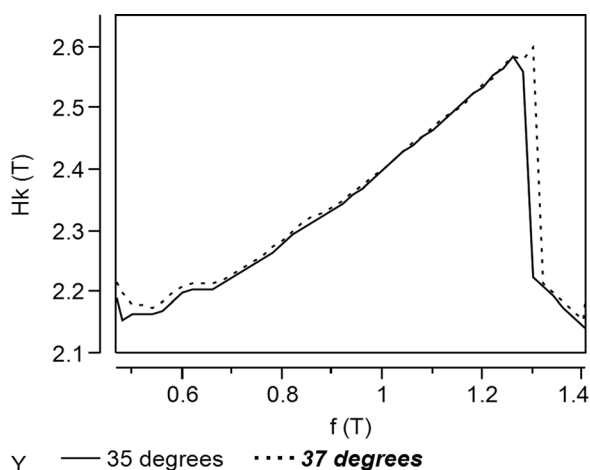
writeability, which occurs almost as a step function of the position in the writer gap, with its magnitude proportional to MAMR H_{eff}, reaching roughly 0.2–0.4 Tesla in majority of proposed recording systems. It occurs at low angles of DC field, since the MAMR frequency varies greatly in this range; it can also occur at high angles of DC field, either when the operating frequency is very high, or the effect is exacerbated by presence of a gradient in RF field amplitude or angle.

The gradient of writeability (i.e., switchable anisotropy values) in conventional magnetic recording is a continuous function of the location within the gap. In MAMR, the derivative of the drop in writeability with respect to location in the gap is almost a delta function. It is localized at a specific point in the gap and occurs at a very specific value of H_k. This means that if during the recording the transition between "positive" and "negative" polarity in the media is formed substantially above or below this value, the impact of MAMR gradient on transition sharpness is absolutely negligible, and such is determined purely by the gradient of the DC field.

Let us now turn to micromagnetic modeling of a more "realistic" writer. There are multiple parameters that determine writer's performance; it appears that for MAMR the most important are the width of the pole perpendicular to the gap (chosen by us to be 20 nm), and the width of the gap (45 nm, although the ones in 20–40 nm range were also modeled). Since we will try to use the same design further on with STO (Spin Torque Oscillator), we did not introduce beveling in the gap, but compensated for its absence with a large, 150 nm tall beveling on the bottom of the write pole at the 45° angle. On the sides, the pole is flared continuously with 35° angle. At the surface facing the recording media (xy plane in Fig. 1), the pole is rectangular and has dimensions of 20 × 80 nm. It should be noted that alteration of any of these parameters does not change conclusions of this manuscript; for a more detailed recording modeling we refer the reader to specialized publications.[10,16] The media

FIG. 6. Maximum reversible anisotropy as a function of frequency for two values of DC field angle.

thickness is taken as 15 nm, with 5 nm spacing between the pole and the media surface. The pole material has saturation magnetization of $4\pi M_s = 2.4$ T. The RF field is uniform, linearly polarized with the magnitude of 0.1 T and applied with angle a in yz plane with respect to the negative direction of z axis and angle b with the positive y axis in the xy plane (Fig. 1).

We calculate the maximum writeable anisotropy in single, decoupled spins placed in the media region, spaced 1 nm away from each other. This limits the amount of writeability gradient we can observe (from spin to spin) to the magnitude of the MAMR effect divided by 1 nm; since such high values were approached, but never actually reached in the modeling, the discretization appears to be sufficient. On the other hand, in a typical recording model, a magnetic grain of 5–10 nm in diameter is used instead of 1×1 nm spins. While we performed such modeling as well, it is quite hard to deduce from it accurate values of writeability gradient and other basic performance parameters, since their impact on recording now strongly depends on the grain diameter, while qualitatively conclusions obtained from such recording model are basically the same. Another complication that appears in a more realistic model is presence of finite exchange coupling—a rather strong one within grain and some limited amount between grains, the latter being quite non-uniform as it depends on the boundary surface between the grains. If the sample size is large enough, a combination of exchange coupling and dipole-dipole interaction can lead to excitation of coupled non-uniform switching, which however requires the area quite larger than the typical bit length in modern magnetic recording (roughly 12.5×60 nm) and therefore probably of little practicality. Another effect is that exchange interaction is quite effective in carrying the absorbed RF fields' energy from one grain to another. Since this effect is similar to the one in conventional recording, in which exchange interaction creates a cluster of grains whose behavior is correlated, resulting in increased bit size and poor confinement of transition between bits, it is reasonable to assume that the same techniques that are used in conventional recording to decrease the intergrain exchange

interaction can be also successfully used in MAMR. Because of these, we decided to limit the presentation in this paper only to an extreme limiting case, which is that of very small, 1 nm in diameter, uncoupled grains. To account for non-uniformity of the DC field, we subdiscritized the media with 1 nm spacing along the media thickness.

Let us calculate the maximum writeable anisotropy in the media as a function of a and b angles (Fig. 7). We see that the micromagnetic writer model (Fig. 7, left) shows the results that are qualitatively the same as those obtained for a single spin in a uniform 1 T DC field at 45° angle (Fig. 7, right), despite the fact that in the first case the DC field is strongly non-uniform and substantially larger in amplitude. Second, the peak H_k value in Fig. 7 falls off as cosine of mismatch with the optimal angles ($a = 70°$, $b = 0°$), essentially repeating the result presented in Fig. 4; the difference in the optimal angle itself from the case of a single spin is mostly explained by the choice of writer design: while yielding a substantially strong DC field amplitude, this particular one produces the best writing at a relatively low angle—36°. The maximum achievable MAMR $H_{eff} = 0.604$ T is also consistent with Eq. (7).

Let us now study how the value of reversible anisotropy H_k changes within the gap. The problem is similar to the one considered in Fig. 5, but now instead of DC field angle the distance y from the write pole edge is changed. The results, demonstrated in Fig. 8 are qualitatively similar to those previously shown in Fig. 5: there is a large drop in writeability for small y (i.e., low DC field angle), and a drop in writeability for large y (i.e., high DC field angle), which occurs only for sufficiently high frequencies. The location of the jumps fits well the Eq. (8), since as we described before they are characteristic of the operating frequency being equal to the largest or optimal MAMR frequency for the given DC angle.

So, there are two large gradients of writeability; it is customary in magnetic recording to refer to the one occurring close to the write pole (small y values) as the leading edge gradient, since this side leads when the media moves underneath the write pole, and to the other one—as the trailing edge gradient. Their modeled values are presented in Fig. 9;
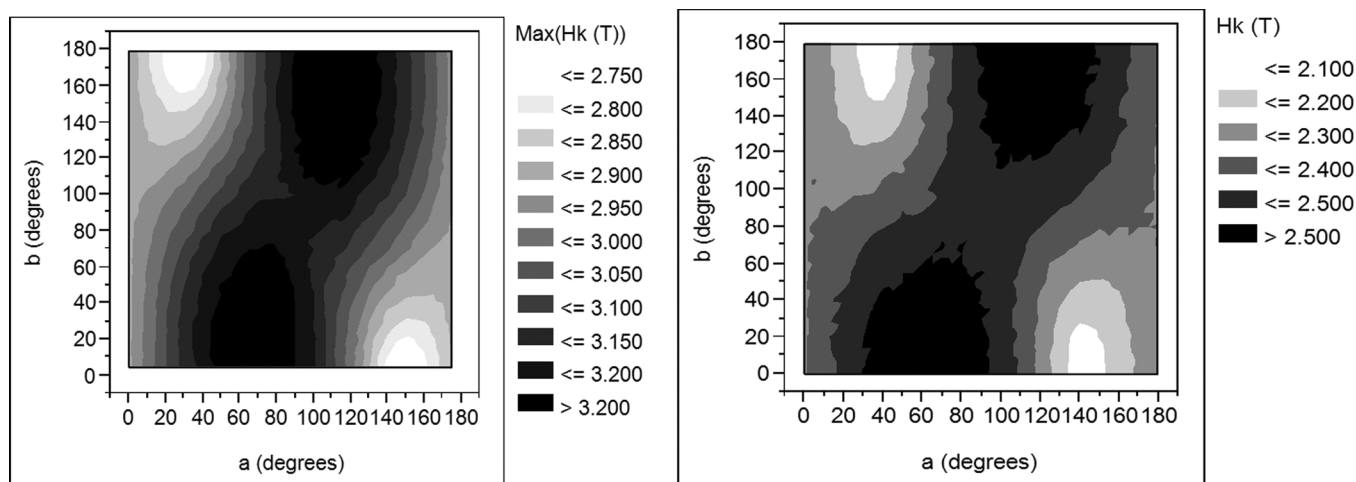

FIG. 7. Maximum writeable anisotropy as a function of RF field angles, obtained with writer model (left) and for a single dipole in the presence of 1 Tesla DC field applied at 45° angle (right).
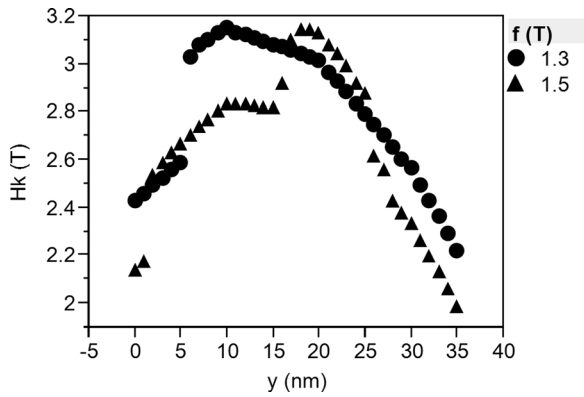
FIG. 8. Maximum reversible anisotropy underneath the pole's center, as a function of coordinate y in the gap, where y = 0 nm is underneath the write pole edge, for two MAMR frequencies f = ω/γ = 1.3 and 1.5 T.

FIG. 10. Track width (TW) in nm as a function of RF field angles, for f = 1.88 T.

as expected, comparison with Fig. 7 shows that the largest gradients are automatically obtained when the peak MAMR effective field is also the largest, and are comparable to its magnitude.

The leading edge gradient is somewhat larger and can be obtained for a much wider range of frequencies—as we have shown before, only at very high frequency the decrease of the optimal frequency at the high angles of the DC field is strong enough to cause a large drop of MAMR effective field on the trailing edge. The values of such frequencies and that of corresponding H_k can either be obtained from numerical modeling or directly from Eqs. (7) and (8).

Let us now briefly consider a question we so far neglected—what happens with the written track in the direction perpendicular to the gap, i.e., on the sides of the pole? To understand this, we return to Figure 7. Suppose we apply the RF field so that around the pole's center, in the writer gap, it is at the optimal angles a and b, the latter is being essentially zero. In this case in the gap, we get a substantial amplification of writeability due to the MAMR effect. But on the sides of the pole, i.e., when x coordinate is greater than the pole width, the DC magnetic field is going to be oriented mostly along x axis (Fig. 1) and therefore almost perpendicular to the RF field, so that the b angle is going to increase to 90°. It is clear from Fig. 7 that for b + 90° the

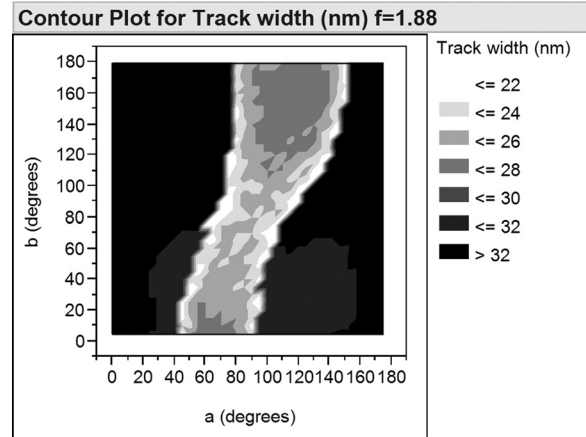MAMR effect is negligible: the angle dependency of MAMR is such that one can choose to enhance the effective field in the recording gap, but not to impact the recording that occurs with the fields parallel to x axis. Therefore, we would expect that a track width, which we can customary define as the width at which the writeable anisotropy is only 85% of its peak value—to decrease due to MAMR. This can be confirmed in the modeling (Figure 10). Here the minimum obtainable track width is 21 nm, close to the pole width of 20 nm, while without MAMR the track width is 34 nm: a well designed MAMR system automatically decreases the track width to the value close to that of the pole width. This means that in order to obtain a very narrow MAMR track the pole should be designed with a small width next to the gap and large flare angles on the sides, along x axis—in this case the field along the track's center will still be amplified by MAMR, but the stray fields parallel to x axis will remain unchanged and therefore the track width will be pushed towards being defined by the pole width alone.

When the RF field is generated by means of a wire, it is relatively easy to adjust the RF angle in the gap by changing the wire placement vis-à-vis the write pole, but it might be complicated to generate the fields with frequencies higher than 20 GHz. To solve this issue, one needs to again address
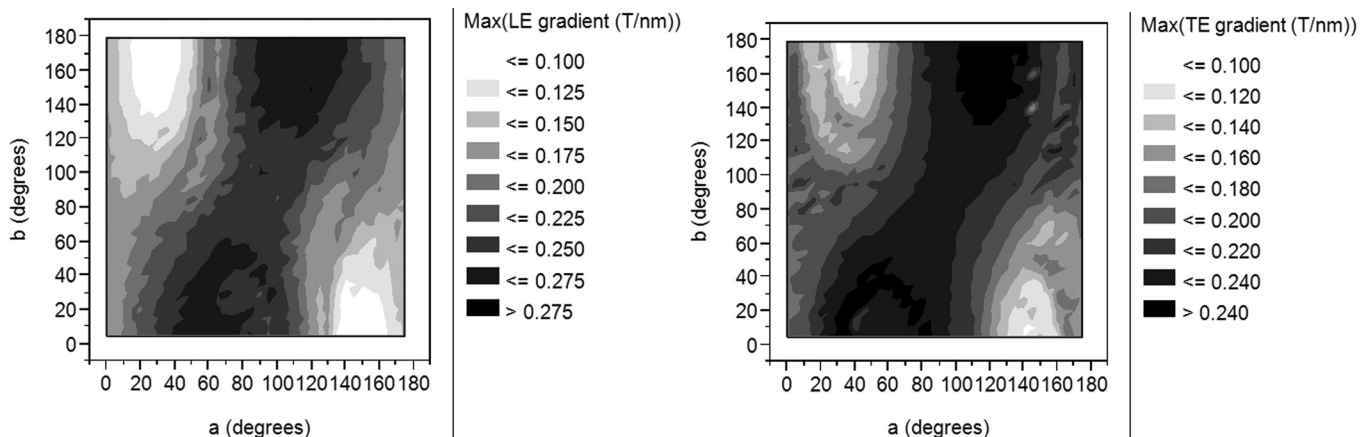

FIG. 9. Writeability gradients on the leading edge (LE), i.e., on the left side of the writer gap, and on the trailing edge (TE), i.e., on the right side of the gap.

the Eq. (8), designing the writer which operates at relatively low angles of DC field, decreasing RF field amplitude and adjusting the RF field angle, allowing one to move the MAMR frequencies into 15–20 GHz range, however at expense of performance.

Let us now consider the case when the RF field is generated by means of spin-torque oscillator (STO, Fig. 11), inserted in the writer gap—a proposal which has been a subject of multiple publications.[16] Such device operates by means of resonant precession of a magnetic layer under the influence of spin torque. In the first order approximation, one can imagine a uniformly magnetized rectangular box (i.e., field generating layer of STO) placed in the gap. For a conventional design, in the absence of current through STO, its magnetization would align roughly parallel to the external field, i.e., along the y axis. Under the influence of spin torque, it rotates (as shown in Fig. 11) around the equilibrium direction. If the external field and equilibrium configuration are parallel to the y axis, rotation occurs clockwise around y axis, if anti-parallel—counter-clockwise, as determined by the precession term in Landau-Lifshitz equation. Rotation occurs in xz plane (Fig. 11), and at each quarter of its oscillations' period consequently the surfaces parallel or perpendicular to the recording media (i.e., along xy or yz planes) acquire a significant magnetic charge (proportional to the component of magnetization along z and x axis respectively), creating fields in the media. These fields also rotate clockwise or counter-clockwise depending on orientation of STO equilibrium magnetization and on their location with respect to the STO (to the left or to the right).

The RF field generated in the gap is very non-uniform, both in terms of its amplitude and its angle with respect to media's anisotropy axis. Let us take a rather typical setup, in which the field generating layer is 13 nm thick, 30 nm wide, and 35 nm tall (we also modeled other dimensions and the conclusions obtained remain unaffected by any reasonable particular choice), $4\pi M_s = 1 T$. Increasing saturation magnetization linearly increases the amplitude of the RF field, and therefore—the magnitude of MAMR effect. However, the choice of STO materials is limited by other considerations, among them is that we need to have effectively around 10 KOe anisotropy in the field generating layer to enable 25–35 GHz operating STO frequency; this can be achieved by either exchange coupling the STO with a high anisotropy material, resulting in a precessing magnetization which is
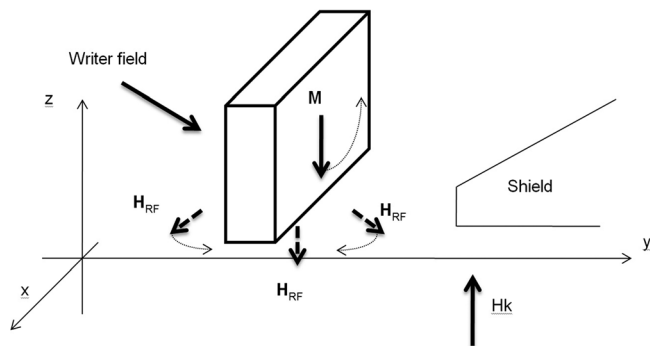
non-uniform along STO thickness (y axis), or by choosing a material with intrinsically high anisotropy; in both cases the saturation magnetization will decrease.

As we mentioned before, the RF field in the media can assume a rather complicated form, but along the center line of the STO (which in most designs corresponds to the center of the recording track), it can be greatly simplified. When magnetic charge along xy planes of STO reaches maximum, the x component of the RF field directly below the center of STO is zero, while the amplitude in yz plane—significant. When yz planes are "charged," the field at the same point is aligned purely along x axis. It means that the RF field can be described with just three numbers—either the amplitude of RF field along y, z and x axis (noting the phase shift between them), or with the amplitude in yz plane H_{yz}, angle it forms with respect to z axis a and the amplitude along x axis H_x,

$$\mathbf{H}_{RF}(t) = \mathrm{Re}\left(e^{-i\omega t} \cdot (\hat{y}H_{yz}\sin a - \hat{z}H_{yz}\cos a \pm i\hat{x}H_x)\right). \quad (9)$$

If the amplitudes of these fields—in yz plane and along x axis are equal, the RF field is circularly polarized. While this can occur at a certain point, almost everywhere in the media it is elliptically polarized; direction of rotation (clockwise or counterclockwise) determines whether the positive or negative sign is used.

We choose to assume that the entire media stack (15 nm, with further 5 nm separation from STO surface) precesses in phase along its thickness, in which case we can use the value of DC and RF fields averaged along its thickness. If we were to operate with very thin media, a considerably higher values of the RF field would be at our disposal, since the field amplitude decays quickly as we move away from the STO (Fig. 12); to a limited extent this can be harnessed by using media layers with varying anisotropy and possibly placing the hardest layer on top,[11,17] but we reserve the discussion of this for a separate paper since the benefits obtained will be in addition to those outlined below.

As one can see from Fig. 12 in general case, the amplitude of the RF field in yz plane is substantially larger than the one along x axis. It is due to the STO surface in xy plane being the only one in the direct proximity towards the media. While circular polarization (i.e., $H_{yz} = H_x$) might be observed at a single point in the media for a specific distance from the STO surface, the MAMR recording occurs also everywhere else; so, we need to extend the Eq. (7) to the case of elliptically polarized field. To do so, we need to return to the step in which we previously replaced the circularly polarized field with two linearly polarized components. Now the amplitudes of these components (in yz plane and x axis) are unequal—if the RF field is circularly polarized one of them is zero, if linearly—both are of equal amplitude

$$H_k \approx H_{SW} + |5.8(H_{yz}|\cos \Delta a| \pm 0.8 H_x)|, \quad (10)$$

$$\frac{\omega}{\gamma} \approx -1.63 H_{RF} + 0.72(H_{SW} - H_0 \cos \phi) + H_{eff}. \quad (11)$$

This formulation is intuitive, as it is essentially a summation of Eq. (8) for various components. If the rotation direction of the RF field is clockwise in the frame of

FIG. 11. A typical design with STO in the gap between the write pole and the shield. Only the field generating layer is shown.
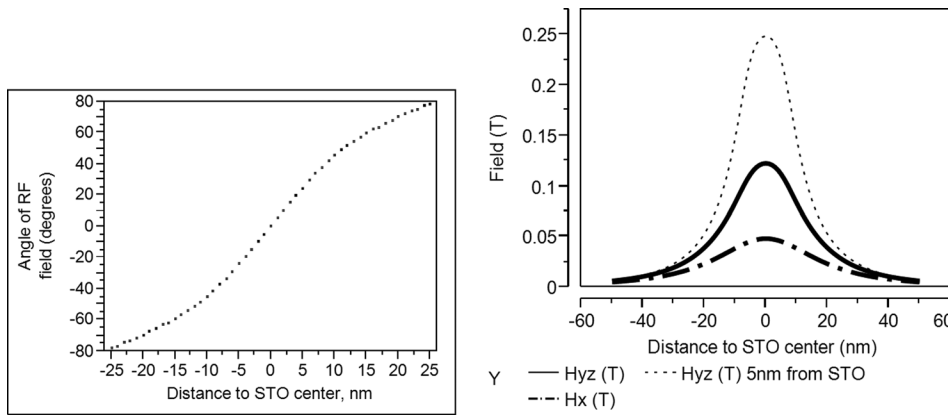
FIG. 12. Characteristics of RF field produced by STO: its angle with respect to anisotropy axis (positive–parallel to the direction of DC field) and the amplitudes of its components along x axis and in yz plane—averaged along the media thickness (thick line) and at 5 nm from the STO surface (dotted thin line).

reference associated with the media's initial direction of the magnetization (such as to the left from the STO in Fig. 11)—the interference between the x and yz components is constructive and the plus sign in Eq. (10) should be used, otherwise their interference is destructive (on the right side from the STO in Fig. 11) and H_x should be subtracted, reducing the effective MAMR field. The coefficient of 0.8 in front of H_x alludes to the fact that for the DC field applied at a substantial angle (from $30°$ to $80°$), the RF field along x axis, i.e., with the angles $a = 0°$, $b = 90°$, does not act as well as the one applied at the optimal angle (Fig. 7). The correction has a weak dependence on the DC field angle, becoming 1 when it approaches 0; overall its impact is small and can be in most cases omitted. For a specific case when the optimal angle a is around $57°$ (i.e., the DC field is between $40°$ and $80°$), by calculating the numerical values of $\cos a$ and $\sin a$ and taking care of the polarization and the consequent choice of sign before the x-component, Eq. (10) simplifies to

$$H_k \approx H_{SW} + |5.8(-0.83H_y + 0.54H_z + 0.8H_x)|. \quad (12)$$

Let us check these equations by observing the effect the STO fields have when the writer field is uniform with amplitude 1 T, applied at $45°$ angle with z axis in the direction opposite to that of initial magnetization state, which is aligned with positive z axis. We study two cases—in the first the STO equilibrium magnetization is parallel to y axis (along the DC field) and its magnetization precesses clockwise around it; in the second it precesses in the counter-clockwise direction (i.e., the equilibrium magnetization is anti-parallel to the DC field). As we did before for linearly polarized

uniform RF field, we calculate the best achievable $H_{eff} = H_k - H_{SW}$ and corresponding operating STO frequency, comparing the results with those calculated from the RF field components directly using Eqs. (10) and (11).

The results are provided in Fig. 13. As we can see, the analytics is rather sufficient; in the first case (clockwise rotation of STO magnetization) the polarization enhances the writing before the STO, but the angle between RF and DC fields there is disadvantageous; while on the right, even though the polarization is disadvantageous, we have an enhancement as the RF angle is optimal (i.e., almost parallel to the DC field). In the second case (counter-clockwise rotation) both effects occur on the right side of the STO, resulting in a very strong writing. Directly underneath the STO in either case the MAMR effect is negligible since the RF field angle is highly suboptimal; in either case the most potent writing occurs almost exactly at the right edge of the STO ($+6$ nm), where even though the total RF field amplitude is less than in its center ($y = 0$ nm), the RF field angle is close to the optimal $60°$ (Fig. 12). For clockwise rotation of STO magnetization, the peak writeability on the left side is shifted away from the STO (-12 nm)—it can be easily deduced from Eq. (10) that the z component of the RF field in this case greatly hampers the recording, and therefore one needs larger RF field angles (Fig. 12).

If the writer DC field is to reverse its direction, so will the equilibrium magnetization of the STO, the direction of magnetization rotation and the initial orientation of media magnetization that we attempt to switch. In the new configuration, the results will be identical to (Fig. 13), as
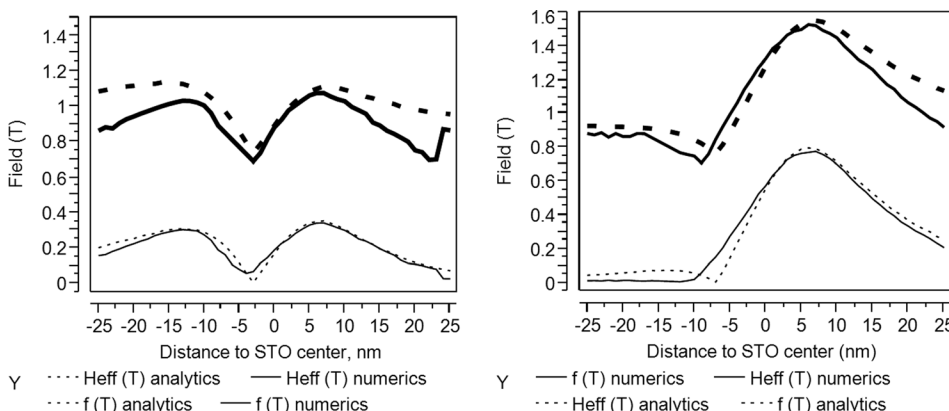

FIG. 13. STO MAMR effective field (thin lines) and optimal frequencies (thick lines): numerical modeling (solid) and analytics (dashed); clockwise (left) and counterclockwise (right) polarities of STO are being considered.
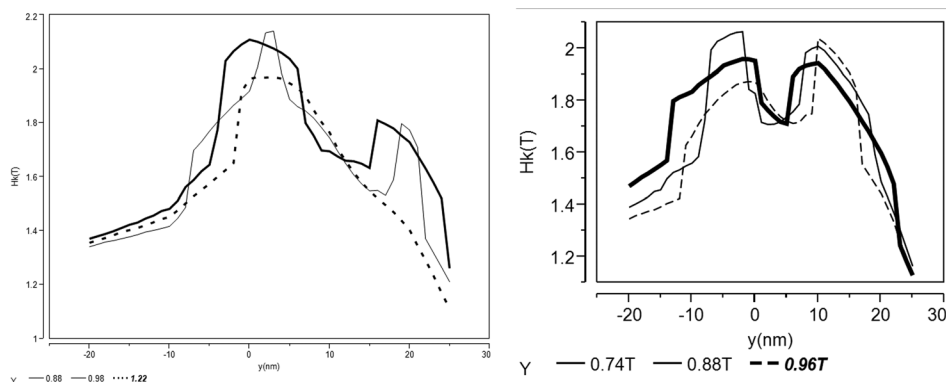
FIG. 14. Writable anisotropy along the STO center with varied placement of STO field generating layer (left—at y = 7 nm distance from the writer edge, right—directly in the contact with the writer edge) and varied frequencies f.

Landau-Lifshitz equation is symmetric with respect to such transformation and as before (Fig. 13, left graph) the fields to the left of STO will have the "beneficial" direction of rotation, but not the angle of the RF field—and on the right the MAMR effect will rely on a more linearly polarized component of the RF field, albeit applied at almost the optimal angle.

The results shown in Fig. 13 define how the STO recording system should be designed. If one manages to produce the STO which aligns itself against the external field of the writer, an extremely potent recording occurs on its rights side, with the effective field more than 10 times the amplitude of RF field generated by the STO. One then needs to operate at proportionally high frequency (Eq. (11)) gives an order of 40 GHz, depending on the amplitude of the DC field) and make the gap at least as wide as almost twice the STO thickness, so that the DC field angle at its right edge is close to the optimal. For the gradients, there would be a very large one right at the edge of the STO, due to the rapidly varying RF field angle there and resulting variation in MAMR effect (Fig. 13), reaching 0.4 T/nm for the given configuration.

However, the case when STO magnetization is aligned along the writer field is more practical, even though the recording process associated with it—is more complex and less advantageous. From Eq. (10), it follows that the ideal STO design is then either the one that writes only on its right side with a linearly polarized field, or the one which writes only on its left side with circularly polarized field. Unfortunately, it can be easily shown that in either it is hard to substantially enhance a basic design, the one considered in this work, by simply adjusting the STO dimensions. The only outcome of such optimization is that the best performing STO is the one with thicker field generating layer, i.e., stronger RF field.

If we now consider a micromagnetic model of both writer and STO, the results will be again consistent with those in Fig. 13: now we have to deal with two separate areas with large MAMR effect, on the left and on the right of the STO (Figures 14 and 15).

By adjusting the gap size, operating frequencies (Fig. 14) and location of STO (Fig. 16), one can boost the write-ability in either of these areas, but still the other one will remain to a potential erasure source. One can also move a point at which the peak writing occurs by selecting the corresponding value of operating frequency (Fig. 13), for

example—to match the peak MAMR gradient with the value at which the transition is written in the media.

There are also two design solutions—the one with writing on the left, between the STO and the write pole, and writing on the right—at the edge of the STO. Both have their advantages. The second design has a somewhat stronger and more localized effective field, but its best gradient is formed on the leading edge—between the center of the STO and its right edge, and it might be difficult to align peak DC writer field with the right edge of STO.

The first design has comparable leading and trailing edge gradients, first formed by both changes in the DC field angle and decay of the RF field, and second formed mostly by the changes in the RF field angle. The writing occurs away from the STO, so this limits the values of the write gap that can be used.

For the second design, regarding the optimal STO width, as one can see in (Fig. 16) for the narrow write pole we use in the modeling (20 nm), wider STO produce larger RF field and therefore larger gradient along the y axis, but it also increases the track width, leaving the optimal STO width to be in 30–40 nm range. The best STO to the write pole distance is rather small. Similar results can be obtained for the first design—and it appears that in some cases one will end up with two (Fig. 15) written areas, both with relatively high gradient.

And, as expected, when MAMR effect is activated (Fig. 15, middle) by choosing the appropriate frequency, the track
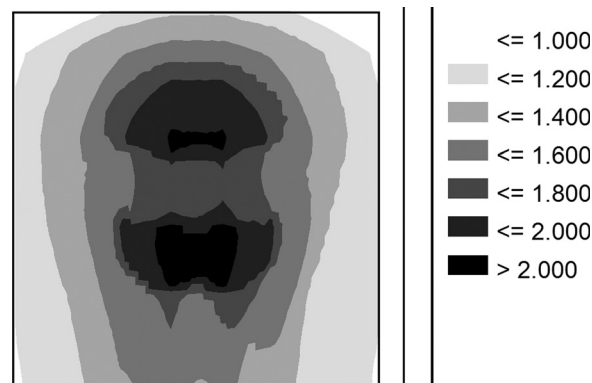

FIG. 15. Typical picture of writable anisotropy in xy plane underneath the write pole at a fixed frequency (f = 0.88 or approximately 25.5 GHz). Two dark areas are separate by the STO.
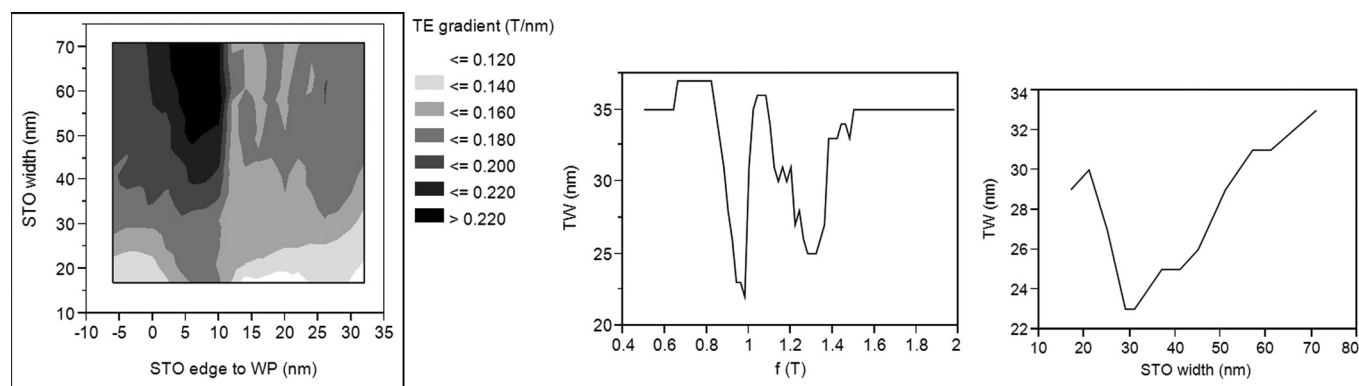
FIG. 16. Peak trailing edge gradient as a function of distance between the STO and the write pole and STO width (left), track width as a function of STO frequency (in Tesla) for STO width equal to 30nm and placement 5nm away from the write pole (middle), and the lowest achievable track width as a function of the STO width for the frequency f = 1 T, STO 5 nm away from the write pole (right).

width rapidly decreases as one utilizes the same effect that we observed before for the uniform RF field—at the optimal MAMR conditions the track collapses to either the pole width, or that of the STO, whichever is smaller, though practical implementation of the system with the combination of wide writer pole and narrow STO requires extraordinary potent MAMR effect.

To conclude this article, we should mention the limitations of this work. While the analytics appears to be on a rather solid ground and compares well both with much more complete numerical models and simple experiments, the recording performance still strongly relies on whether the MAMR gradient can be reliably converted into improved transition quality. While it is possible to achieve this in various recording models, in practice the outcome will be affected by a multitude of phenomena which are hard to simulate with sufficient precision. For example, the stable oscillation of the STO can be established only after both the write pole and the shield are fully reversed and produce fields with amplitudes similar to the steady state solution. This means that RF field is generated after the static field already reached its maximum, and unless the STO field is very strong and media anisotropy is considerably high, it is possible that because of the distributions in the media, some of the grains are already switched or about to do so—and the MAMR gradient has therefore limited impact on the written transition. Whether it happens or not depends on nuances of media dynamics, which today cannot be directly measured in experiment. A wire generated RF field would not have this issue. Optimizing the STO design by maximizing the gradients and effective field given by Eqs. (10) and (11) yields a more potent system than the simple ones considered in this work.

[1]C. Thirion, W. Wernsdorfer, and D. Mailly, Nature Mater. **2**, 524–527 (2003).

[2]G. Bertotti, C. Serpico, and I. D. Mayergoyz, Phys. Rev. Lett. **86**, 724 (2001).

[3]K. Rivkin, N. Tabat, and S. Foss-Schroeder, Appl. Phys. Lett. **92**, 153104 (2008).

[4]K. Rivkin and J. B. Ketterson, Appl. Phys. Lett. **89**, 252507 (2006).

[5]S. Okamoto, I. Igarashi, N. Kikuchi, and O. Kitakami, J. Appl. Phys. **107**, 123914 (2010).

[6]M. Furuta, S. Okamoto, N. Kikuchi, O. Kitakami, and T. Shimatsu, Appl. Phys. Express **6**, 053006 (2013).

[7]Y. Nozaki, N. Ishida, Y. Soeno, and K. Sekiguchi, J. Appl. Phys. **112**, 083912 (2012).

[8]C. Nistor, K. Sun, Z. Wang, M. Wu, C. Mathieu and M. Hadley, Appl. Phys. Lett. **95**, 012504 (2009).

[9]S. Okamoto, N. Kikuchi, A. Hotta, M. Furuta, O. Kitakami, and T. Shimatsu, Appl. Phys. Lett. **103**, 202405 (2013).

[10]T. Tanaka, S. Kashiwagi, Y. Furomoto, Y. Otsuka, and K. Matsuyama, Nanoscale Res. Lett. **8**, 461 (2013).

[11]Y. Nozaki, A. Kato, K. Noda, Y. Kanai, T. Tanaka, and K. Matsuyama, J. Appl. Phys. **109**, 123912 (2011).

[12]V. Tiberkevich and A. Slavin, Phys. Rev. B **75**, 014440 (2007).

[13]M. J. Hurben and C. E. Patton, J. Appl. Phys. **83**, 4344 (1998).

[14]I. Mayergoyz, *Mathematical Models of Hysteresis and their Applications* (Academic Press, 2013).

[15]S. Okamoto, N. Kikuchi, and O. Kitakami, Appl. Phys. Lett. **93**, 102506 (2008).

[16]J. Zhu, X. Zhu, and Y. Tang, IEEE Trans. Magn. **44**, 125 (2008).

[17]K. Rivkin and N. Tabat, "Microwave assisted magnetic recording system," U.S. patent 20,090,262,457 A1 (2008).

[18]A. Shukh and N. Tabat, "Writer for perpendicular recording with controlled write width," U.S. patent 6,954,340 (2005).

[19]D. Wilton, D. McKirdy, H. Shute, J. Miles, and D. Mapps, IEEE Trans. Magn. **40**, 148 (2004).

[20]M. Mallary, A. Torabi, and M. Benakli, IEEE Trans. Magn. **38**, 1719 (2002).